Habit Modification of the API Lovastatin through a Predictive Solvent Selection Approach

T. D. Turner*[1], L. E. Hatcher[2], C. C. Wilson[2], K. J. Roberts[1]

[1]*Centre for the Digital Design of Drug Products, School of Chemical and Process Engineering, University of Leeds, Woodhouse Lane, Leeds, LS2 9JT*

[2] *Future Continuous Manufacturing and Advanced Crystallisation (CMAC) Research Hub, Department of Chemistry, University of Bath, Bath BA2 7AY*

** Corresponding Author*

Keywords

Molecular Modelling, Synthonic Engineering, Surface Chemistry, Morphology Prediction, Lattice Energy, Lovastatin

Declarations of interest: none

Abstract

An analysis of the important intermolecular interactions of the active pharmaceutical ingredient (API) lovastatin which contribute to the surface chemistry and attachment energy morphology is presented. The analysis is supported by a recent redetermination of the single crystal structure (orthorhombic space group $P2_12_12_1$) and targets the understanding and potential control of the morphology of lovastatin, which tends to crystallise in a needle-like morphology, where the aspect ratio varies depending on the nature of the solvent. The lattice energy was calculated to be -38.79 kcal mol^{-1} with a small contribution of -2.73 kcal mol^{-1} from electrostatic interactions. The lattice structure is significantly stabilised by the hexahydronaphthalene ring of the molecule, which contributes 43.39 % of the lattice energy. Synthon analysis shows that the dominant intermolecular interaction within the lattice structure of lovastatin is found to be along the a crystallographic axis, associated with a dispersive stacking interaction due to the close packing of two hexahydronaphthalene rings resulting in a total energy of -6.46 kcal mol^{-1}. The attachment energy morphology correlates well with the observed crystal morphology which exhibits a needle-like habit dominated by {0 1 1}, {0 2 0}, {0 0 2} and {1 0 1} crystal forms. The needle capping faces are found to contain the short stacks of hexahydronaphthalene rings where the strong intermolecular synthon is found to contribute positively to the attachment energy and hence growth at this surface. This dominant intermolecular synthon is concluded to be the major cause of enhanced growth along the crystallographic a axis leading to the formation of a needle-like morphology. A habit modification strategy is discussed which uses recrystallization from a-polar solvents to reduce the effective growth rate at the needle capping surfaces. This is supported through experimental data which shows that crystals

obtained from crystallisation in hexane and methyl-cyclohexane have significantly reduced aspect ratios in comparison to those grown from methanol and ethyl acetate solutions. Crystals obtained from nitromethane solutions were found to have a very large reduction in aspect ratio to a prismatic morphology, critically with no polymorph change.

Introduction

Mevinolinic acid or lovastatin belongs to the statin class of drug compounds, one of the most widely prescribed drug classes worldwide for the treatment of hypercholesterolemia. Lovastatin targets and inhibits the enzyme hydroxymethylglutaryl coenzyme A reductase (HMG-Co A), which plays a key role in initiating the synthesis of cholesterol, hence lovastatin hinders the biosynthesis pathway of cholesterol. Lovastatin is generally isolated through a chemical synthesis or biosynthesis fermentation route, where the product is then isolated and purified through a re-crystallization strategy, generally from alcohol or acetone/water mixes[1].

Lovastatin has been the target of many physicochemical screening studies within the literature due to its importance as an industrial active pharmaceutical ingredient (API). The solid state physicochemical properties of lovastatin have been studied utilising thermal analysis methods; the melting point was found to be 445 K and where the crystalline material undergoes amorphization when recrystallized with the preservative butylhydroxyanisole[2]. The solubility of lovastatin was measured in a number of solvent systems; namely in a series of homologous acetates[3], alcohols[4] and also in acetone/water mixtures[5], where the solubility is lower in polar solvents due to the hydrophobic nature of the compound. Additionally the nucleation kinetics of lovastatin have been determined using turbidometric techniques in ethanol,

methanol and acetone solutions; where the mechanism of nucleation was found to be instantaneous in ethanol and acetone and progressive in methanol[4].

Due to the hydrophobicity of lovastatin, the drug falls into the second class of drug compounds under the Biopharmaceutics Classification System (BCS), [6] [7] where the drug exhibits high permeability and low solubility, the molecular structure and material descriptors for lovastatin are provided in S1 of the ESI. As a result the drug is impacted by poor bioavailability and hence efforts to improve the absorption of the drug have included nanoparticle synthesis and implementation of lipid based carrier systems[8, 9]. Lovastatin also exhibits a needle-like morphology when recrystallized from solution, which can lead to problematic downstream processing issues such as poor particle flow, problematic filtration and particle breakage[10].

The physicochemical and mechanical properties of crystalline materials can be calculated using molecular modelling tools through atom-atom summation methods which utilize atomistic forcefields to calculate intermolecular interaction strength and directionality[11] [12] [13] [14] [15] [16] [17]. Much progress has been made in this field, particularly when applying these 'synthonic engineering' methodologies to organic molecular crystals[18] [19], where particle morphology[20] [21], solvent-surface interactions[22], surface chemistry[23] and excipient-API interactions[24] are some of the emerging areas of interest. Nguyen[25] et al recently applied a synthonic engineering approach to understand the interfacial stability of the crystallographic faces of ibuprofen and rationalise the various aspect ratio crystals obtained from differing solution environments during crystal growth. Rosbottom[26] and co-workers have also utilised synthonic engineering by applying a grid-based surface searching methodology[27] [28] [29] [30] to explain the anisotropic wettability of the crystal surfaces of ibuprofen.

This paper aims to utilise the approaches of synthonic engineering and molecular modelling discussed above to further understand the bulk crystal chemistry and surface chemistry of lovastatin in relation to its observed needle-like morphology. Additionally it aims to quantify the extrinsic (surface terminated) synthon contribution to the attachment of molecules at the growing crystal surfaces. This is part of an overall strategy to effect the habit modification of this material to mitigate the impact of the observed needle-like morphology of lovastatin by providing a fundamental molecular understanding of both the crystallographic structure and the nature of the interactions of the solute with its surrounding solution environment.

Materials and Methods

Chemicals

Lovastatin was used as supplied by through the EPSRC Future Continuous Manufacturing and Advanced Crystallisation (CMAC) Research Hub, and originally purchased through Molekula. Ethyl acetate HPLC >99.95%, methanol HPLC 99.61%, hexane HPLC 99.9% purity was used as supplied by Fisher. Toluene reagent grade >99.7%, methyl cyclohexane anhydrous >99% was used as supplied by Sigma Aldrich.

Experimental Methodology

Single Crystal X-ray Diffraction

Single crystals of lovastatin (colourless needles) were obtained by slow evaporation from saturated ethyl acetate, methanol, methyl cyclo-hexane, toluene, hexane and nitromethane solutions at 25 °C. Single crystal X-ray diffraction data were recorded at the University of Bath, on a dual source Rigaku Oxford Diffraction Gemini A Ultra

diffractometer, equipped with an Atlas CCD detector and an Oxford Cryosystems Cryojet-XL liquid nitrogen flow device for temperature control. Data collection, indexing and integration procedures were performed using the Rigaku Oxford Diffraction software CrysAlis Pro[31]. Using Olex2[32], the structure was solved by dual space methods using ShelXT[33] and refined by Least Squares methods using ShelXL[34]. Hydrogen atoms were positioned geometrically and refined using a riding model. The hydrogen atom isotropic displacement parameters were fixed to U_{iso}(H) = 1.5 x (for CH3) or U_{iso}(H) = 1.2 x (for CH2 and CH) the U_{eq} of the parent atom. The structure is included in the Cambridge Structural Databases as a CSD Communication with CSD refcode CEKBEZ01[35].

Powder X-ray Diffraction

Powder x-ray diffraction was used for polymorph characterisation of the prepared lovastatin crystals from slow solvent evaporation. The powder samples were ground to a powder using a mortar and pestle then mounted on a single cut silicon crystal powder holder and scanned using a Bruker[36] D8 advanced X-ray diffractometer using Cu Kα radiation and a germanium primary monochromator in Bragg-Brentano reflection geometry. The step size was 0.033 2θ with a step time of 0.7 s/step over a 2θ range of 2-39.8 2θ. The detector used was a Vantec-1 position sensitive detector.

Modelling Methodology

Visualisation of the crystal structure was carried out using the Cambridge Crystallographic Data Centre's (CCDC) Mercury software[37]. The conformational analysis of lovastatin (CEKBEZ01)[35] was performed using the Forcite module in Accelrys Material Studio[38] where the geometry of a single lovastatin molecule of the

major disorder component, was optimised with respect to the potential energy surface to minimise the total energy of the structure. The PCFF[39 40 41] forcefield was used and the atomic charges were calculated using Gasteiger[42 43], the energy convergence was calculated using the SMART algorithm. The geometry of this gas phase optimised molecule of lovastatin was then compared to the conformation of the molecule in the crystal structure.

The lattice, slice and attachment energies were calculated using an atom-atom summation method using Habit98[44 45] using the Momany[46] potential where the atomistic charges were calculated within Mopac[47]. Habit98 builds a series of unit cells which expand outward from a central unit cell, the intermolecular interaction between a central molecule and all others within an expanding sphere, the radius of which was set as 1 – 30 Å to ensure lattice energy convergence, are calculated. The resulting lattice energy was partitioned into the slice and attachment energy based on Equation 1[48].

$$E_{cr} = E_{sl} + E_{att} \quad (1)$$

$$\varepsilon_{hkl} = \frac{E_{sl}}{E_{cr}} \quad (2)$$

Where E_{cr} is the lattice energy, E_{sl} is the slice energy and E_{att} is the attachment energy. The important morphological faces were selected based upon the Bravais, Friedel, Donnay and Harker (BFDH) rule[49 50 51] which states the surfaces with lowest surface energy will be those with the greatest inter-planar d-spacing and were chosen using the Morphology tool with Materials Studios. The predicted morphology was calculated using the top 10 crystal planes sorted by the highest d-spacing where the attachment energy of those faces was calculated and the attachment energy was approximated to a surface-specific growth rate. The morphology was then

reconstructed using a Wulff plot using SHAPE[52 53]. The surface anisotropy factors[54 55], ε_{hkl}, which describe the termination of the synthons at a specific habit face, were calculated using Equation 2 and expressed as a percentage. The plane rugosity of the crystal faces were calculated based on the average route mean square displacement of the atomic centres of the molecules in the unit cell along the growth normal within the d-spacing of the crystallographic planes. The plane rugosity provides a simple measure of the variation in height for a given crystallographic plane and hence provides a description of the smoothness for a given crystal plane at an atomic level. The intermolecular synthons were analysed and ranked by their total intermolecular energy contribution to the overall lattice energy of lovastatin following a methodology previously reported by Rosbottom et al[17].

Results

Single Crystal Structure Determination

The single crystal structure of lovastatin (CSD refcode CEKBEZ) was first published by Sato *et al.* in 1984 and was determined from room temperature X-ray diffraction data.[56] The data presented in this paper are a modern redetermination of the structure at low temperature (150 K), confirming that the overall structure of lovastatin remains largely unchanged on cooling, the crystal structure refinement data of lovastatin is provided in S2 of the ESI. No structural phase transition is observed on cooling, with the same $P2_12_12_1$ space group retained at 150 K and slightly reduced unit cell parameters, as is in-keeping with thermal contraction on cooling (overall decrease in unit cell volume = *c.a.* 2%). An overlay of the two structures in the CSD software Mercury[57] confirms that the molecular conformation is largely unchanged on cooling, with a RMS deviation of 0.0214 calculated between

the two structures (see ESI, S2 Figure 2). The key difference between the new structure and that published by Sato *et al.* is that disorder in the *S*-butanoate ester group was resolved at low temperature. The *S*-butanoate group is found to be disordered over two positions and was freely refined using standard PART instructions to determine a ratio of 57% of the major component and 43% of the minor component (see ESI S2 Figure 3). The conformation of the major component overlays well with the reported room temperature arrangement for this group (see ESI S2 Figure 2). Although no disorder was reported by Sato *et al.,* analysis of their original structure data does show that the anisotropic displacement parameters (ADPs) for the *S*-butanoate chain are significantly larger than for the rest of the structure (for example, the reported ADP for the carbon atom of the terminal CH_3 group is *c.a.* 2 x larger than that of other CH_3 groups in the structure).[56] These observations indicate that the presence of disorder cannot be entirely ruled out in the room temperature structure, and are thus consistent with our own observations at low temperature. It should also be noted that the data quality is also remarkably improved in the 150 K redetermination, with a residual factor R1 = 3.17% in comparison to R1 = 8.2% for the original dataset. A reduction in data quality at room temperature is common,[58] and hence may reasonably have prevented reliable refinement of any potential disorder in the structure collected in 1984. Given this comparison, we chose the 150 K redetermination as the basis for our molecular modelling calculations which were performed using the major component, however for clarity the methodology was repeated using the minor component where the data is comparable and the conclusions drawn from this analysis are in agreement; this is provided in S3 of the ESI.

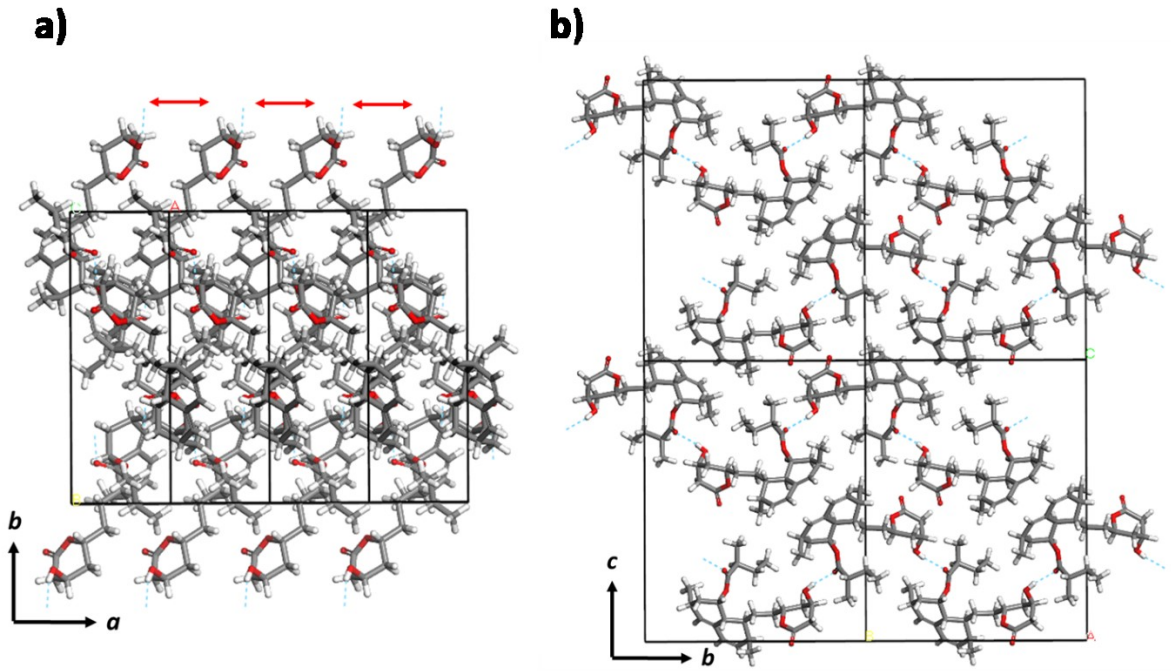

Figure 1 a) the crystal structure of lovastatin viewed down the crystallographic *c* axis highlighting the close stacking of the hexahydronaphalene rings (red arrows) along the *a* axis and b) view down the crystallographic *a* axis highlighting the hydrogen bond between the *S*-butanoate ester group and the alcohol functionality

Figure 1a) provides a view of the lovastatin crystal structure down the *b* axis which highlights the close packed nature of the hexahydronaphthalene rings which run down the short *a* axis of the crystal structure. The crystal structure contains one hydrogen bond between the alcohol functionality and the carbonyl of the *S*-butanoate ester group. These interactions form a broken chain which runs ~30° from plane normal down the crystallographic *b* axis. Additionally there is a notable short contact between the carbonyl group of the tetrahydropyran ring and an acidic proton on an adjacent tetrahydropyran ring which runs ~20° from plane normal to the crystallographic *a* axis, an enlarged view of this contact is provided in S4 of the ESI.

Conformational Analysis

The calculated gas phase conformation of a lovastatin molecule is shown as yellow in Figure 2 and is overlaid for comparison to the conformation of the molecule in the asymmetric unit found in the crystal structure, coloured by atom type in Figure 2. The data shows that in general the conformation of the lovastatin molecule does not change dramatically when going from the gas phase to the crystal structure. This is particularly observable in the conformations of the hexahydronaphthalene and the S-butanoate ester groups, which exhibit very little conformational change. The torsion around the carbon back bone highlighted as red T1 in View A, Figure 2 highlights this small change which only differs by ~1°, 172° - 171° when going from the gas phase to the crystalline phase. The tetrahydropyran ring group, however, does undergo some conformational rotation when going from the gas phase to the solid phase, where the ring is rotated ~ 23°, 154° – 177°, through torsion T2 highlighted in green in View B, Figure 2. The total energy of the molecule within the crystal structure was found to be -19.70 kcal mol^{-1} and the optimised gas phase molecule had a total energy of -20.82 kcal mol^{-1}, which correlates well with a small conformational change. Overall this analysis is consistent with the material only having a single known polymorph; where the crystal structure conformation is already relatively close to the molecular free energy minima.

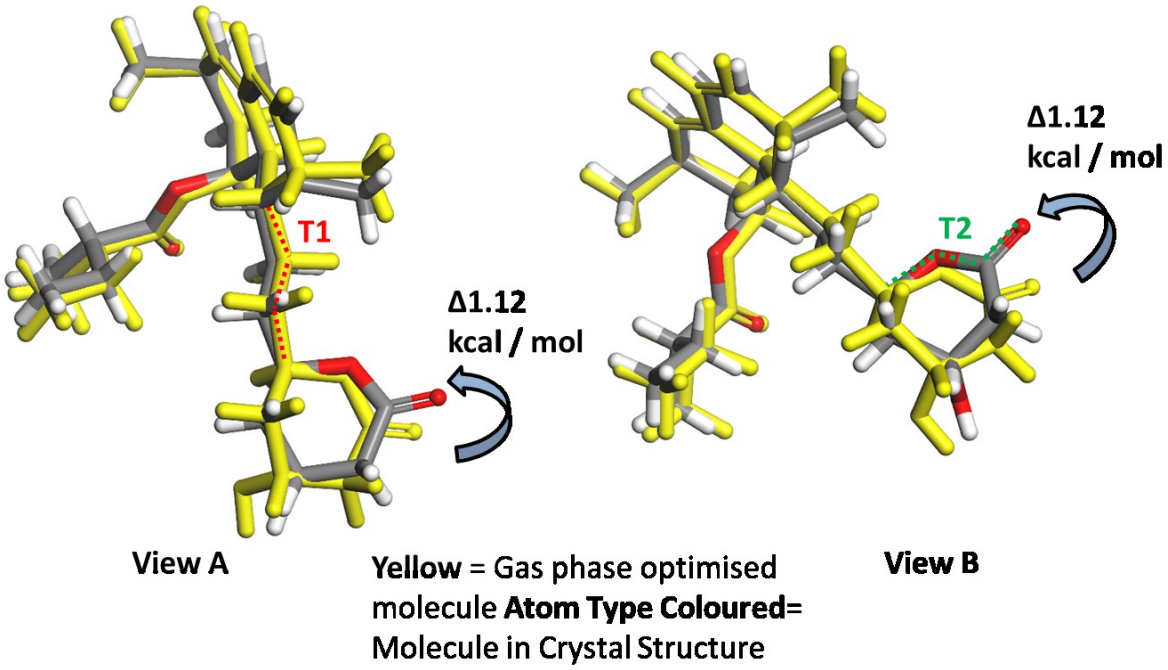

Figure 2 Conformational overlay of the gas phase optimised lovastatin molecule (yellow) and the molecule in the asymmetric unit of lovastatin (coloured by atom type) highlighting the conformational change of the tetrahydropyran ring through torsion 2 (T2 Green)

Lattice Energy and Intermolecular Synthon Analysis

The lattice energy of lovastatin converged at -38.79 kcal mol^{-1} where the electrostatic contribution converges at -2.73 kcal mol^{-1} at a maximum convergence distance of 30 Å. The lattice energy and electrostatic contribution energy as a function of limiting radius are provided in Figure 3a), this shows that the lattice energy converges in two shell's, the first at 6 – 9 Å and the second at 13 Å as shown in Figure 3b). The very low contribution to the lattice energy provided by electrostatic interactions is unsurprising considering the largely dispersive nature of the lovastatin molecule.

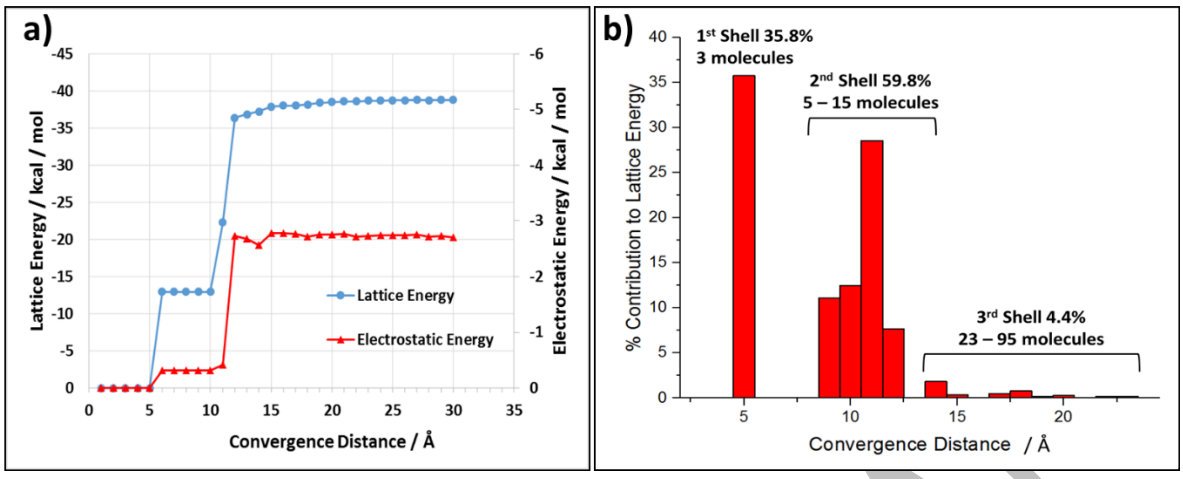

Figure 3 a) Convergence of the calculated lattice total energy as a function of limiting radius for lovastatin, also indicating the contribution made to this by the electrostatic interactions, b) the % contribution to the lattice energy as a function of convergence distance, indicating the three shells via which the lattice energy of lovastatin converges together with the number of molecules in the shell

The lattice energy of lovastatin was further collapsed onto the asymmetric molecular unit to provide a quantitative analysis of the relative functional group contribution to stabilising the crystal lattice. Figure 4a) provides this quantitative breakdown onto the lovastatin molecule where the hexahydronaphthalene group (*α*) contributes 43.39 % of the lattice energy, indicating the importance of dispersive interactions within the lovastatin lattice structure. The tetrahydropyran functionality (*β*) contributes 29.42 % and the *S*-butanoate ester group (*γ*) contributes 27.24 %, interestingly the β group contains the acidic proton short contact between the carbonyl group of the tetrahydropyran ring and the protons of an adjacent tetrahydropyran ring. Whereas the *γ* group contains the long range H-bond (~2.0 Å) from the ester functionality, this highlights the subtle differences between the H-bonding component and the short contact component to the lattice energy where the acidic proton short contact seems to play a greater role in contributing to the stabilisation of the lattice structure.

Figure 4b) summarises the top seven intermolecular synthons, ranked by intermolecular interaction energy, which contribute to the lattice energy of lovastatin, additionally Table 1 summarises the breakdown of these synthonic interactions into

attractive, repulsive, coulombic and total energy from the force field calculation. Synthon A provides the largest contribution to the lattice energy of lovastatin, -6.46 kcal/mol and 33.31% of the total lattice energy, ~ 3.5 kcal/mol greater than synthon B which highlights the importance of this close packed interaction which is ~98% dominated by dispersive interactions between the hexahydronaphthalene groups as summarised in Table 1. Synthons B and E contain a larger coulombic component, ~20% and 26% contribution to the overall interaction respectively. This is due to the hydrogen bond between the alcohol proton and carbonyl oxygen in synthon B and the acidic proton short contact in synthon E as shown in Figure 4b). Synthons F and G provide a relatively small contribution to the overall crystal lattice energy with weak dispersive type interactions of -1.05 and -0.92 kcal/mol respectively. These seven synthons provide 93.06% of the total lattice energy of lovastatin and hence analysis of further intermolecular synthons was not carried out due to their low contribution to the overall lattice energy.

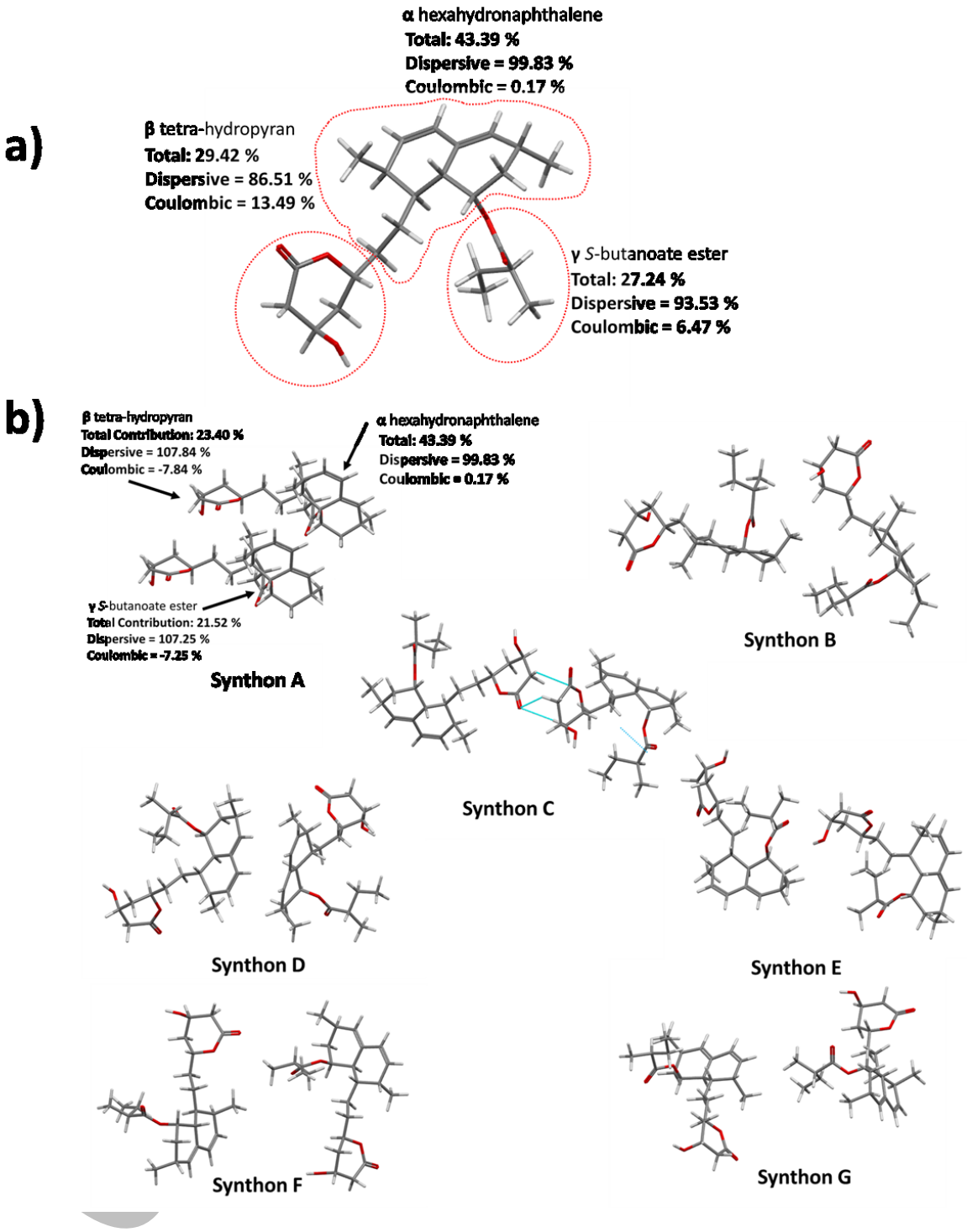

Figure 4 a) The percentage contribution to the lattice energy provided by the 3 functional groups of the lovastatin asymmetric unit, and the breakdown of each to dispersive and coulombic contribution to the total, b) The top seven intermolecular synthons which contribute to the lattice energy of lovastatin, ranked as a function of total interaction energy, Synthon A shows the breakdown of the total contribution of the three main functionality's (as identified in a)) of the lovastatin molecule towards the overall intermolecular interaction energy together with the percentage contribution of the dispersive and coulombic components of those functionality's

Table 1 The top seven intermolecular synthons which contribute to the lattice energy of lovastatin, ranked in order of total interaction energy, also provided is the contribution of each synthon to the total lattice energy and also the contributions in multiplicity of synthons to the surfaces present in the attachment energy morphology

Synthon	*Distance/Å	Dispersive Total kcalmol^{-1}	Coulombic kcalmol^{-1}	Total kcalmol^{-1}	% Contribution of Lattice Energy	Contribution to Attachment Energy {0 1 1}	Contribution to Attachment Energy {0 2 0}	Contribution to Attachment Energy {1 0 1}
A	5.89	-6.31	-0.16	-6.46	33.31	0	0	4
B	11.11	-2.47	-0.50	-2.98	15.36	2	4	3
C	10.35	-2.58	0.02	-2.56	13.20	2	4	1
D	10.03	-2.04	-0.08	-2.12	10.93	2	4	2
E	11.39	-1.45	-0.51	-1.96	10.11	2	4	2
F	11.11	-0.92	-0.13	-1.05	5.41	2	0	2
G	11.91	-0.90	-0.01	-0.92	4.74	2	0	2
					Total = 93.06 %			

**Distance is calculated from the centre of gravity of the two molecules contributing to the intermolecular interaction*

The strongest intermolecular synthon, Synthon A, comprises of a close stacked interaction of the hexahydronaphthalene rings. Figure 4b) provides a schematic of Synthon A with the breakdown of the interaction energy onto the functional groups of lovastatin. This shows that the hexahydronaphthalene rings provide 54.66% of the interaction energy and the β and γ functional groups provide 23.40% and 21.52% respectively. Further to this, it was found that the components of this intermolecular interaction energy is dispersive in nature as highlighted by the breakdown of the energy into dispersive and coulombic components as highlighted in Table 1.

Attachment Energy Morphology and Surface Chemistry

The attachment energy morphology of lovastatin is provided in Figure 5 where the simulation yields a needle-like morphology dominated by {0 1 1}, {0 2 0}, {1 0 1} and {0 0 2} surfaces; where the {1 0 1} surfaces are the needle capping faces. The calculated attachment energy morphology is in reasonably good agreement with micrographs of lovastatin crystals grown from ethyl acetate and toluene solutions,

shown in Figure 6 which present as needle-like crystallites albeit of a higher aspect ratio in comparison to the model morphology, a more detailed figure of the calculated attachment energy morphology is provided in S5 in the ESI.

Table 2 summarises the slice, attachment energy and % surface saturation of the top 10 BFDH face list of lovastatin, where the highlighted faces are those which are present in the calculated attachment energy morphology. Interestingly the % surface saturation of the morphologically important surfaces, correlates well to the morphology, whereby the needle capping surfaces, {1 0 1}, have by far the lowest surface saturation, 30.21%, meaning growth in this direction would be favoured due to unsatisfied surface active intermolecular interactions. Conversely the slow growing {0 1 1} surface has the highest surface saturation, 66.69%, meaning growth is likely to be slower in this direction.

Table 2 The calculated slice and attachment energies together with the % surface saturation of the top 10 BFDH face list for lovastatin, the major surfaces which appear in the calculated attachment energy morphology are highlighted

Surface	d Spacing / Å	Plane Rugosity / Å	Slice Energy / kcal mol^{-1}	Attachment Energy / kcal mol^{-1}	% Surface Saturation
{0 1 1}	13.61	7.22	-25.87	-12.91	66.69
{0 2 0}	8.66	5.88	-17.43	-21.35	44.93
{1 0 1}	5.69	2.61	-11.72	-27.06	30.21
{0 0 2}	10.99	6.09	-25.3	-13.48	65.22
{0 1 2}	9.28	7.26	-23.75	-15.04	61.23
{0 2 1}	8.06	6.69	-20.59	-18.2	53.08
{0 1 3}	6.75	7.08	-23.71	-15.07	61.12
{0 3 1}	5.59	6.44	-15.38	-23.41	39.65
{0 2 3}	5.6	7.34	-23.71	-15.07	61.12
{1 1 0}	5.6	3.41	-11.83	-26.95	30.50

The overall contribution of the top five intermolecular synthons, presented in Figure 4, to the attachment energy of the {0 1 1}, {0 2 0} and {1 0 1} surfaces was calculated to assess the relative importance to the growth of these faces. This analysis is summarised in Table 1 where the multiplicity of each synthon is presented. This analysis shows that, interestingly, the needle capping {1 0 1} surface is the only morphological surface to contain synthon A as an extrinsic growth synthon. This correlates well with the observation that the morphology is extended down the a axis through this surface. Conversely the larger, slower growing {0 1 1} surface has no contribution from synthon A to its attachment energy and only has the lower energy synthons B, C, D and E with a multiplicity of 2, as extrinsic synthons.

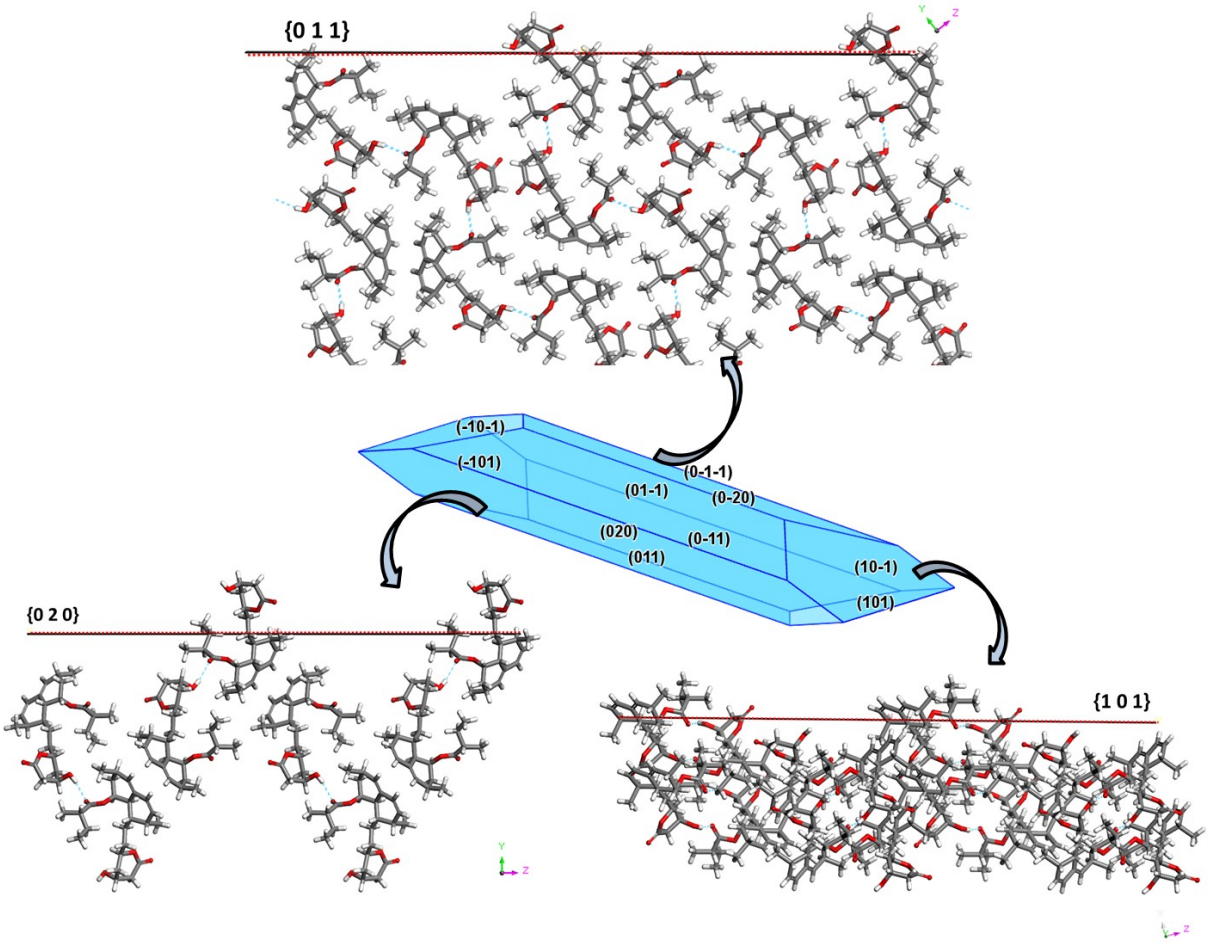

Figure 5 Attachment energy morphology of lovastatin together with a visualisation of the surface chemistry of the morphologically important faces; {0 1 1}, {0 2 0} and {1 0 1}

A visualisation of the surface chemistry for the {0 1 1}, {0 2 0} and {1 0 1} surfaces of lovastatin is provided in Figure 5. This indicates the closed packed nature of the {1 0 1} needle capping surface and shows the relative availability of the hexahydronaphthalene rings at the surface which can provide stacking interactions to form the energetically favourable synthon A, which was highlighted in the previous analysis, and contributes to the attachment energy at this surface. Additionally the calculated plane rugosity (Table 2) of the {1 0 1} surface was found to be 2.61 Å which is low relative to the {0 1 1} and {0 2 0} surfaces. This could provide a more favourable growth environment, whereby de-solvation of the surface followed by

solute integration is to some extent less rate limited by the de-solvation step due to solvent trapping at the surface for example. Conversely the {0 1 1} and {0 2 0} surfaces have significantly higher calculated plane rugosity than the needle capping surface, which could impact de-solvation; where the channels trap solvent and hence decrease the rate of de-solvation and effectively decrease the growth rate at these surfaces relative to the needle capping surface.

Synthonic and Surface Chemistry Analysis in Relation to the Needle Morphology of Lovastatin

This analysis has indicated the importance of Synthon A, not only in contributing to the stabilisation of the lattice structure of lovastatin but also to the attachment energy as an extrinsic synthon on the needle capping {1 0 1} surface. The combination of a highly favourable dispersive stacking interaction between the two hexahydronaphthalene groups, the low calculated {1 0 1} plane rugosity and the availability of the hexahydronaphthalene groups at the capping surface are the likely cause of the formation of a needle-like morphology due to faster crystal growth along the crystallographic *a* axis of lovastatin.

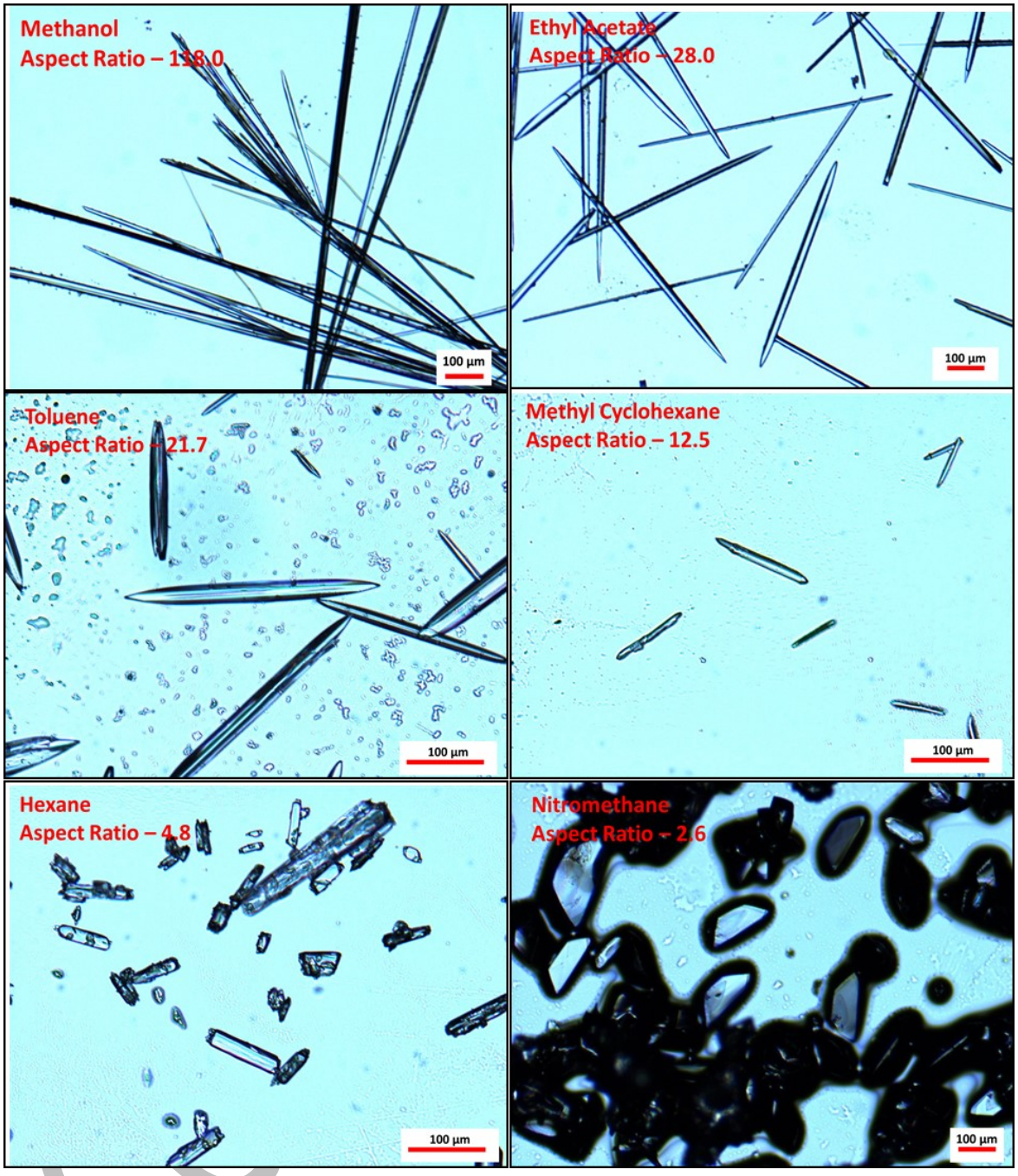

Figure 6 Micrographs of lovastatin crystals grown by slow solvent evaporation from, methanol (aspect ratio 118.0), ethyl acetate (aspect ratio 28.0), toluene (aspect ratio 21.7), methyl cyclohexane (aspect ratio 12.5), hexane (aspect ratio 4.8) and nitromethane solutions (aspect ratio 2.6), the approximate aspect ratio of the crystals were calculated by the ratio of the approximate length and width of the crystals

The identification of Synthon A, not only as an important possible growth synthon, but also as an extrinsic synthon at the needle capping face, leads to the postulation of a crystallisation strategy to hinder or at least reduce the aspect ratio of the crystals through selective binding of the hexahydronaphthalene rings to hinder formation of

Synthon A. Micrographs of lovastatin crystals obtained from slow solvent evaporation in some non-polar solvents are provided in Figure 6. This highlights that in methyl cyclohexane, toluene, hexane and nitromethane solutions, the crystallites recovered had a significantly lower aspect ratio when compared to those grown in polar protic or polar a-protic solvents such as methanol and ethyl acetate. This is likely due to selectively binding of the a-polar component of the lovastatin molecule which would effectively decrease the de-solvation rate of the molecule at the hexahydronaphthalene group in the solution state, hindering the formation of Synthon A and also decrease the de-solvation rate of the {1 0 1} capping face relative to the side and top faces. This reduction in relative growth rate would likely decrease the aspect ratio to a more equant morphology.

Nitromethane provides an interesting result as this solvent considerably reduces the aspect ratio of the lovastatin crystals to a prismatic-like morphology. The crystals obtained were analysed for polymorph changes, where powder x-ray diffraction showed the crystals to be the same crystal structure and hence no polymorph change or solvate formation had taken place, this data is provided in S6 of the ESI. The cause of this dramatic reduction in needle-like morphology is likely to be the prevention of Synthon A formation and the reduction of the growth rate on the needle capping face. This dramatic habit modification has also been shown for the case of *p*-aminobenzoic acid (PABA), where the needle-like alpha form can be reduced to a significantly more prismatic crystal habit through recrystallization from nitromethane solutions. This was found to be caused by interaction of nitromethane with the benzene ring of PABA and hence disrupting an important π-π stacking interaction which causes the needle-like morphology in the material. This is also likely the case for lovastatin, where the nitromethane could preferentially bind to the

hexahydronaphthalene ring system, probably through the unsaturated carbon atoms, and hence prevent Synthon A formation.

The effect of 'blocking' Synthon A using solvation could also be similarly achieved through additive addition using the same principle. Additives such as poly-aromatic or poly-cyclic hydrocarbons e.g. naphthalene, could have the same effect by blocking Synthon A and also through disruption of the molecular recognition at the {1 0 1} capping surface, reducing the effective growth rate.

Conclusions

A molecular modelling analysis of the intrinsic and extrinsic synthons of the API lovastatin in relation to its bulk and surface properties has been presented to rationalise the materials' observed needle-like morphology. The synthonic analysis revealed a strong intermolecular interaction in the bulk structure which consisted of a close packed stacking interaction of two hexahydronaphthalene rings. This intermolecular interaction was found to be ~ 3.5 kcal mol^{-1} more energetically favourable than the second strongest synthonic interaction in the bulk structure. Additionally the hexahydronaphthalene ring of lovastatin was found to contribute 43.39 % of the calculated lattice energy of the material, where 99.83% of this was found to be of a dispersive nature.

The calculated attachment energy morphological model correlated reasonably well with the experimental morphology observed for crystals grown from ethyl acetate solutions, and was dominated by {0 1 1}, {0 2 0}, {1 0 1} and {0 0 2} surfaces. Analysis of the surface chemistry of the habit faces revealed that the {1 0 1} needle capping face was under-saturated with respect to its extrinsic synthons, where the surface saturation was calculated as 30.21%, compared to 66.69 % and 44.93 % for

the {0 1 1} and the {0 2 0} surfaces respectively. The {1 0 1} needle capping face also was found to have a lower plane rugosity, 2.61 Å, compared to 5.88 Å and 7.22 Å for the {0 2 0} and {0 1 1} faces respectively. The analysis of the surface chemistry revealed that critically, Synthon A contributes positively to the attachment energy of the {1 0 1} capping surface, and does not contribute to the attachment energy of either the {0 2 0} and {0 1 1} faces. Hence it was concluded that Synthon A is the major cause for the formation of a needle-like morphology in lovastatin down the crystallographic *a* axis and a recrystallization strategy using a-protic or a-polar solvents or additives could be used as habit modifiers for this material to reduce the aspect ratio of the crystals.

Acknowledgements

This work was funded by the Advanced Manufacturing Supply Chain Initiative 'Advanced Digital Design of Pharmaceutical Therapeutics' (ADDoPT) project (Grant No. 14060). This work also builds upon research on morphological modelling supported by EPSRC grant 'HABIT – Crystal morphology from crystallographic and growth environment factors' through EPSRC grant EP/I028293/1 and the Synthonic Engineering programme supported by Pfizer, Boeringer-Ingellheim, Novartis and Syngenta. We also gratefully acknowledge EPSRC for the support of crystallization research at Leeds and Manchester through the Critical Mass grant 'Molecules, Clusters and Crystals' (Grant references EP/IO14446/1 and EP/IO13563/1). We are grateful to the EPSRC for the financial support of the Future Continuous Manufacturing and Advanced Crystallisation (CMAC) Research Hub (Grant EP/P006965/1).

List of Symbols

E_{cr}	Lattice energy / kcal / mol
E_{sl}	Slice energy / kcal / mol
E_{att}	Attachment energy / kcal / mol
ε_{hkl}	Anisotropy factor
R_{int}	Merging residual factor (crystallography): $\frac{\sum\left\|F_o^2 - F_o^2(mean)\right\|}{\sum\left[F_o^2\right]}$
R_{sigma}	Signal-to-noise residual factor (crystallography): $\frac{\sum[\sigma F_o^2]}{\sum\left[F_o^2\right]}$
R_1	Conventional residual factor (crystallography): $\frac{\sum\left\|\|F_o\| - \|F_c\|\right\|}{\sum\|F_o\|}$
wR_2	Weighted residual factor (crystallography): $\sqrt{\frac{\sum w(\|F_o\|^2 - \|F_c\|^2)^2}{\sum w\|F_o\|^2}}$
ρ_{calc}	Calculated density (crystallography)
U_{eq}	Equivalent isotropic atomic displacement parameter
U_{iso}	Isotropic atomic displacement parameter
Z	Number of formula units within the crystallographic unit cell

References

1 Mulder KCL, Mulinari F, Franco OL, Soares MSF, Magalhães, BS, Parachin NS. Lovastatin production: From molecular basis to industrial process optimization. Biotechnology Advances 2015;33:648–665.

2 Yoshida MI, Oliveira MA, Gomes ECL, Mussel WN, Castro WV, Soares CDV. Thermal characterization of lovastatin in pharmaceutical formulations. J Therm Anal Calorim 2011;106:657–664

3 Nti-Gyabaah J, Chiew YC. Solubility of Lovastatin in Acetone, Methanol, Ethanol, Ethyl Acetate, and Butyl Acetate between 283 K and 323 K. J Chem Eng Data 2008;53:2060–2065

4 Zhang X, Yang Z, Chai, J.; Xu, J.; Zhang, L.; Qian, G.; Zhou, X. Nucleation kinetics of lovastatin in different solvents from metastable zone widths. Chemical Engineering Science 2015;133:62–69

5 Sun H, Wang J. Solubility of Lovastatin in Acetone + Water Solvent Mixtures. J Chem Eng Data 2008;53:1335–1337

6 Amidon GL, Lennerhas H, Shah VP, Crison JR. A theoretical basis for a biopharmaceutic drug classification: the correlation of in vitro drug product dissolution and in vivo bioavailability. Pharm Res 1995;12:413–20

7 Amidon K.S, Langguth P, Lennernäs H, Yu L, Amidon GL. Bioequivalence of oral products and the biopharmaceutics classification system: science regulation and public policy. Clin Pharmacol Ther 2011;90:467–470.

8 Chen CC, Tsai TH, Huang ZR, Fang JF. Effects of lipophilic emulsifiers on the oral administration of lovastatin from nanostructured lipid carriers: physicochemical characterization and pharmacokinetics. Eur J Pharm Biopharm 2010;74:74-82.

9 Seenivasan A, Panda T, Théodore T. Lovastatin Nanoparticle Synthesis and Characterization for Better Drug Delivery. The Open Biotechnology Journal 2011;5:28-32.

10 Variankaval N, Cote AS, Doherty MF. From form to function: Crystallization of active pharmaceutical ingredients. AIChE J 2008;54:1682–1688.

11 Hartman P, Bennema P. The attachment energy as a habit controlling factor: I. Theoretical considerations. J Cryst Growth 1980;49:145−156.

12 Clydesdale G, Docherty R, Roberts KJ. HABIT - a program for predicting the morphology of molecular crystals. Comput Phys Commun 1991;64;311–328.

13 Clydesdale G, Roberts KJ, Docherty R. HABIT95 — a program for predicting the morphology of molecular crystals as a function of the growth environment. J Cryst Growth 1996;166:78–83.

14 Clydesdale G, Roberts KJ, Walker EM. The crystal habit of molecular materials: A structural perspective, In *Molecular Solid State: Syntheses, Structure, Reactions, Applications*, 1996

15 Docherty R, Clydesdale G, Roberts KJ, Bennema P. Application Of Bravais-Friedel-Donnay-Harker, Attachment Energy And Ising-Models To Predicting And Understanding The Morphology Of Molecular-Crystals. J Phys D: Appl Phys 1991;24:89−99.

16 Docherty R, Roberts KJ. Modelling The Morphology Of Molecular-Crystals - Application To Anthracene, Biphenyl And Beta-Succinic Acid. J Cryst Growth 1988;88:159−168.

17 Rosbottom I, Roberts KJ, Docherty R. The solid state, surface and morphological properties of p-aminobenzoic acid in terms of the strength and directionality of its intermolecular synthons. Cryst Eng Comm 2015;17:5768−5788.

18 Desiraju GR. Supramolecular Synthons in Crystal Engineering A New Organic Synthesis. *Angew* Chem Int Ed Engl 1995;34:2311−2327.

19 Roberts KJ, Hammond RB, Ramachandran V, Docherty R. Synthonic engineering: from molecular and crystallographic structure to the rational design of pharmaceutical solid dosage forms. In *Computational Approaches in Pharmaceutical Solid State Chemistry*, Abramov, Y., Ed.; Wiley: New Jersey, USA, 2016.

20 Hammond RB, Pencheva K, Ramachandran V, Roberts KJ. Application of grid-based molecular methods for modelling solvent dependent crystal growth morphology: Aspirin crystallized from aqueous ethanolic solution. Cryst Growth Des 2007;7:1571−1574.

21 Hammond RB, Ramachandran V, Roberts KJ. Molecular modelling of the incorporation of habit modifying additives: [small alpha]-glycine in the presence of l-alanine. Cryst Eng Comm 2011;13:4935−4944.

22 Hammond RB, Pencheva K, Roberts KJ. A Structural− Kinetic Approach to Model Face-Specific Solution/Crystal Surface Energy Associated with the Crystallization of

Acetyl Salicylic Acid from Supersaturated Aqueous/Ethanol Solution. Cryst Growth Des 2006;6:1324−1334.

23 Hammond RB, Pencheva K, Roberts KJ. Molecular modelling of crystal-crystal interactions between the alpha- and beta polymorphic forms of L-glutamic acid using grid-based methods. Cryst Growth Des 2007;7:875−884.

24 Ramachandran V, Murnane D, Hammond RB, Pickering J, Roberts KJ, Soufian M, Forbes B, Jaffari S, Martin GP, Collins E, Pencheva K. Formulation Pre-screening of Inhalation Powders Using Computational Atom−Atom Systematic Search Method. Mol Pharmaceutics 2015;12:18−33.

25 Nguyen TTH, Rosbottom I, Marziano I, Hammond RB, Roberts KJ. Crystal Morphology and Interfacial Stability of RS-Ibuprofen in Relation to Its Molecular and Synthonic Structure Cryst Growth Des 2017;17:3088−3099.

26 Rosbottom I, Pickering JH, Etbon B, Hammond RB, Roberts KJ. Examination of inequivalent wetting on the crystal habit surfaces of RS-ibuprofen using grid-based molecular modelling. Phys Chem Chem Phys 2018;20:11622-11633

27 Hammond RB, Hashim RS, Ma C, Roberts KJ. Grid-based molecular modelling for pharmaceutical salt screening: Case example of 3,4,6,7,8,9-hexahydro-2H-pyrimido (1,2-a) pyrimidinium acetate. J Pharm Sci 2006;95:2361−2372.

28 Hammond RB, Jeck S, Ma CY, Pencheva K, Roberts KJ, Auffret T. An Examination of Binding Motifs Associated With Inter- Particle Interactions between Facetted Nano-Crystals of Acetylsalicylic Acid and Ascorbic Acid through the Application of Molecular Grid- Based Search Methods. J Pharm Sci 2009;98:4589−4602.

29 Hammond RB, Hashim RS, Ma C, Roberts KJ. Grid-based molecular modeling for pharmaceutical salt screening: Case example of 3, 4, 6, 7, 8, 9-hexahydro-2H-pyrimido (1, 2-a) pyrimidinium acetate. J Pharm Sci 2006;95:2361−2372.

30 Hammond RB, Ma C, Roberts KJ, Ghi PY, Harris, RK. Application of systematic search methods to studies of the structures of urea-dihydroxy benzene cocrystals. J Phys Chem B 2003;107:11820−11826.

31 CrysAlis Pro, Rigaku Oxford Diffraction Data Collection and Data Reduction GUI, Version 171.38.43.

32 Dolomanov OV, Bourhis LJ, Gildea RJ, Howard JAK, Puschmann H. OLEX2: a complete structure solution, refinement and analysis program. J Appl Cryst 2009;42:339-341.

33 Sheldrick GM. Crystal structure refinement with SHELXL. Acta Cryst 2015;A71:3-8.

34 Sheldrick0 GM. A short history of SHELX., Acta Cryst 2008;A64;112-122.

35 Hatcher, 2018, CSD Communication, DOI:10.5517/ccdc.csd.cc1zf0p3

36 https://www.bruker.com/, accessed November 2018

37 Cambridge Crystallographic Data Centre, Cambridge Structural Database, 1965

38 A. S. Inc., San Diego, 5.5 edn., 2011

39 Sun H, Mumby SJ, Maple JR, Hagler AT. An ab initio CFF93 all-atom forcefield for polycarbonates. J Am Chem Soc 1994;116:2978-2987

40 Sun H. Force field for computation of conformational energies, structures, and vibrational frequencies of aromatic polyesters. J Comput Chem 1994;15:752-768.

41 Hill JR, Sauer J. Molecular mechanics potential for silica and zeolite catalysts based on ab initio calculations in Dense and microporous silica. J Phys Chem 1994;98:1238-1244.

42 Gasteiger J, Marsili M. Iterative partial equalization of orbital electronegativity—a rapid access to atomic charges. Tetrahedron 1980;36:3219–3228.

43 Gasteiger J, Marsili M. A new model for calculating atomic charges in molecules. Tetrahedron Lett 1978;34:3181–3184.

44 Clydesdale G, Docherty R, Roberts KJ. HABIT - a program for predicting the morphology of molecular crystals. Comput Phys Commun 1991;64:311-328.

45 Clydesdale G, Roberts KJ, Docherty R. HABIT95 - a program for predicting the morphology of molecular crystals as a function of the growth environment. J Cryst Growth 1996;166:78-83.

46 Momany FA, Carruthers LM, McGuire RF, Scheraga HA. Intermolecular potentials from crystal data. III. Determination of empirical potentials and application to the packing configurations and lattice energies in crystals of hydrocarbons, carboxylic acids, amines, and amides. J Phys Chem 1974;78:1595-1620

47 Mopac, version 6.0: Quantum Chemistry Program Exchange Program No. 455. Creative Arts Building 181, Indiana University, Bloomington, IN 47405

48 Berkovitch-Yellin Z. Toward an ab initio derivation of crystal morphology. J Am Chem Soc 1985;107:8239–8253.

49 Bravais A. Etudes Crystallographiques, Gauthiers Villars, Paris, 1886

50 Donnay JDH, Harker DA new law of crystal morphology, extending the law of Bravais Am Mineral 1937;22:446–467.

51 Friedel G. Étudessurla loi de bravais. Bull Soc Fr Mineral Crist 1907;30:326-455.

52 Bruno IJ, Cole JC, Edgington PR, Kessler M, Macrae CF, McCabe P, Pearson J, Taylor R. New software for searching the Cambridge Structural Database and visualizing crystal structures. Acta Crystallogr Sect B: Struct Sci 2002;58:389–397.

53 Dowty E. Computing and drawing crystal shapes. Am Mineral 1980;65:465–472.

54 Human HJ, Van Der Eerden JP, Jetten LAMJ, Odekerken JGM. On the roughening transition of biphenyl: Transition of faceted to non-faceted growth of

biphenyl for growth from different organic solvents and the melt. J Cryst Growth 1981;51:589–600.

55 Jetten LAMJ, Human HJ, Bennema P, Van Der Eerden JP. On the observation of the roughening transition of organic crystals, growing from solution. J Cryst Growth 1984;68:503–516.

56 Sato S, Hata T, Tsujita Y, Terahara A, Tamura C. The structure of monacolin K, C24H26O5. Acta Crystallographica Section C 1984;40(1):195-198

57 Macrae CF, Bruno IJ, Chisholm JA, Edgington PR, McCabe P, Pidcock E, Rodriguez-Monge L, Taylor R, van de Streek J, Wood PA. Mercury CSD 2.0- new features for the visualization and investigation of crystal structures. Journal of Applied Crystallography 2008; 41(2):466-470

58 Goeta AE, Howard JAK. Low temperature single crystal X-ray diffraction: advantages, instrumentation and applications. Chemical Society Reviews 2004; 33(8):490-500.